FTIR Surface Site Analysis of Pillared Clays Using Pyridine Probe Species

Stephen A. Bagshaw and Ralph P. Cooney*

Chemistry Department, University of Auckland, Private Bag 92019, Auckland, New Zealand

Received February 24, 1993. Revised Manuscript Received May 17, 1993

The surface acidities of alumina-, zirconia-, and titania-pillared clays (montmorillonite, synthetic mica–montmorillonite, and rectorite) and the unpillared parent clays have been studied by infrared spectroscopy using pyridine as a spectroscopic probe species under variable-temperature desorption conditions. These semiquantitative studies of thermally activated pillared clays suggest that the characteristics of surface Lewis acid sites are primarily determined by the pillar species while those of the Brönsted sites are determined by both the pillar species and the parent clay used. Alumina-pillared clays exhibit both Lewis and Brönsted acidity associated with the pillars, while zirconia- and titania-pillared clays exhibit only Lewis acidity on the pillars with Brönsted activity being associated with the exposed clay surfaces and pillar-to-clay layer bonding sites. Relative acid site strengths are estimated by using the extent of retention of pyridine under desorption conditions and by determining the magnitude of adsorption-induced wavenumber shifts for pyridine vibrational bands. The overall acidity of alumina-pillared rectorite was found to be the strongest of the pillared clays studied, while the acidity of zirconia-pillared montmorillonite was the weakest.

Introduction

The vibrational spectrum of adsorbed pyridine is known to be sensitive to the nature of the adsorption site.[1] Site-sensitive bands in the Fourier transform infrared (FTIR) spectrum of adsorbed pyridine have been employed in the determination of ratios of Brönsted (or protonic, B) to Lewis (or coordinative, L) acid sites for various solid oxide surfaces.[2-10] Information relating to these ratios is important in the evaluation of catalytic function of adsorbents.

The structures of clay layers and of PILCs are still the subject of some conjecture. This is primarily due to the wide variations in chemical composition of the layers, the arrangements of the layers themselves, the variability in speciation of pillaring solutions,[11] and the possible arrangements of pillars within the interlayer space. Three clays with different structures were used in the present study; namely, montmorillonite, rectorite, and synthetic mica–montmorillonite. The structure of montmorillonite has often been described in the PILC literature.[8] Rectorite is a uniformly interstratified illite–smectite clay in which the swelling smectitic layers comprise approximately 60% of the clay layers and are largely beidellitic.[12] There are also significant amounts of iron(II) and iron(III) substitution in the octahedral layer as evident in the present work in the red color of the sample wafer after activation. Synthetic mica–montmorillonite is a randomly interstratified mica–smectite clay which can be described as having two-thirds illite-like nonswelling layers and one-third smectite-like (montmorillonitic) swelling layers[13] and no iron impurities. Detailed descriptions and elemental analyses of the structures and properties of these clays can be found in the mineralogical literature[12-14] and are therefore not presented here.

The clay layers themselves are only weakly acidic[15] with active sites being found in the interlayer space at sites of cation exchange and small numbers of acidic OH groups (B sites) found at platelet edges and fracture sites where the octahedral layer hydroxyls are exposed. Therefore a significant increase in acidity would be expected upon the introduction of metal oxy–hydroxy pillaring species into the interlamellar region. Infrared (IR) spectroscopic studies using pyridine and ammonia as adsorbates on pillared montmorillonite and beidellite have been reported[16-20] and reviewed.[21,22] The earlier workers were primarily interested in identifying the types of acid sites on the PILC surfaces and the behavior of these sites in catalytic reactions. Ming-Yuan *et al.*[22] used *n*-butylamine titration, in conjunction with infrared spectroscopy of adsorbed pyridine and ammonia, to analyze the acidic

(1) Parry, E. P. *J. Catal.* **1963**, *2*, 371.
(2) Cooney, R. P.; Curthoys, G.; Tam, N. T. *Adv. Catal.* **1975**, *24*, 293.
(3) Occelli, M. L. *J. Mol. Catal.* **1986**, *35*, 377.
(4) Morterra, C.; Chiorino, A.; Ghiotti, G.; Garrone, E. *J. Chem. Soc., Faraday Trans 1* **1979**, *75*, 271.
(5) Morterra, C.; Coluccia, S.; Chiorino, A.; Boccuzzi, F. *J. Catal.* **1978**, *54*, 348.
(6) Nikiel, L.; Zerda, T. W. *J. Phys. Chem.* **1991**, *95*, 4063.
(7) Ward, J. W. *J. Catal.* **1968**, *11*, 251.
(8) Poncelet, G.; Shutz, A. *Chemical reactions in organic and inorganic constrained systems*; D. Reidel: Dordrecht, 1986; p 165.
(9) Dines, T. J.; Rochester, C. H.; Ward, A. M. *J. Chem. Soc., Faraday Trans 1* **1991**, *87*, 643.
(10) Cardonna-Martinez, N.; Dumesic, J. A. *J. Catal.* **1990**, *125*, 427.
(11) Baes, C. F. Jr.; Mesmer, R. E. *Hydrolysis of Cations*; Wiley: New York, 1976.
(12) Kodama, H. *Am. Mineral.* **1966**, *51*, 1035.
(13) Wright, A. C.; Grandquist, W. T.; Kennedy, J. V. *J. Catal.* **1972**, *25*, 65.
(14) Newman, A. C. D. *Chemistry of Clays and Clay Minerals*; Mineralogical Society, Monograph 6: London, 1987.
(15) Davitz, J. C. *J. Catal.* **1976**, *43*, 260.
(16) Brindley, G. W.; Sempels, R. E. *Clay Miner.* **1977**, *12*, 229.
(17) Occelli, M. L.; Tindwa, R. M. *Clays Clay Miner.* **1983**, *31*, 22.
(18) Plee, D.; Shutz, A.; Poncelet, G.; Fripiat, J. J. *Catal. Acids Bases* **1985**, 343.
(19) Tennakoon, D. T. B.; Jones, W.; Thomas, J. M.; Ballantine, J. H.; Purnell, J. H. *Solid State Ionics* **1987**, *24*, 205.
(20) Diddams, P. A.; Thomas, J. M.; Jones, W.; Ballantine, J. H.; Purnell, J. H. *J. Chem. Soc., Chem. Commun.* **1984**, 1340.
(21) Figueras, F. *Catal. Rev-Sci. Eng.* **1988**, *30*, 457.
(22) Ming-Yuan, H.; Zhonghui, L.; Enze, M. *Catal. Today* **1988**, *2*, 321.

0897-4756/93/2805-1101$04.00/0

characteristics of a variety of PILCs. Their data are consistent with the literature, showing that the acidity of PILCs is largely Lewis type and associated with the pillars and that an increase in acidity occurs with increasing pillar density. However, in that study,[22] as with other studies, no differentiation between pillar and clay-layer sites was made, nor were values for the [B]/[L] acid site ratios quantitatively determined. It has also been demonstrated that both Lewis and Brönsted acidities disappear upon calcination.[21,22] This is in contrast to zeolites where Lewis acidity increases at the expense of Brönsted acidity upon calcination.[23]

The objectives of this investigation have been the evaluation of [B]/[L] ratios for a series of PILCs incorporating a variety of pillar species (viz. oxy–hydroxy species of aluminium, zirconium, and titanium), and the analysis of relative acid site strengths of the various calcined PILCs. It was anticipated that this study would permit adsorption processes on both the internal clay surfaces and the pillar surfaces to be distinguished. Further, it became apparent throughout the course of the study that two different parameters of acid-site strength could be identified. The first relates to the extent of retention of adsorbed pyridine during desorption, while the second is the adsorption-induced wavenumber shift of pyridine vibrational bands. Our results show that the findings emerging from the two different approaches are similar. Furthermore, the preparation, characterization, and surface acid properties of zirconia- and titania-pillared rectorite have not previously been reported.

Experimental Section

Sample Preparation. Samples of Wyoming montmorillonite (SWy-1), Arkansas rectorite (RAr-1), and synthetic mica–montmorillonite (Syn-1) were obtained from the Source Clays Repository, University of Missouri. The montmorillonite and synthetic mica-montmorillonite were used without further purification. The rectorite, as supplied, contained large quantities of quartz, sand, and stone, from which the clay was separated by aqueous dispersion of the clay. The clays were then sodium-exchanged with 6.0 mol L^{-1} NaCl solution and then dialyzed until chloride-free. The pyridine used was a BDH AnalaR product which was stored under vacuum.

The preparation of the pillaring reagents and the pillaring procedures have been previously described.[24,25] These methods were modified for use in the present study. Dialysis was preferred over filtration or centrifugation, for the washing of chloride ions from the PILCs, because it has greater convenience in the separation of the clay and also allows for the possibility of continued cation hydrolysis leading to larger pillar species during the dialysis. It also ensures that the cation-exchange process attains an equilibrium given the length of time the clay suspension is in contact with the pillaring solution.

PILCs with different pillar loadings were synthesized by adding more or less pillaring solution per gram of clay to the aqueous clay dispersion. The PILCs discussed in the text are referred to by labels, for example, Al-M6, meaning Al-pillared montmorillonite containing 6.0 mmol of Al/g of clay. The PILCs were dried in air of 353 K overnight then stored in sealed moisture-proof containers.

The PILCs, as prepared, were characterized using X-ray diffraction (XRD) of oriented films, formed by slow evaporation of the water from a drop of PILC suspension placed on a quartz glass slide. Five-point BET N_2 adsorption surface areas (Table I) were obtained from powdered samples degassed *in situ* at the temperature indicated. Earlier workers[25] have reported difficulty in obtaining unambiguous XRD patterns of titanium-pillared clays. This behavior is observed in the present study and has been ascribed to the presence of a wide range of polymer species in the pillaring solution[11] causing the nonuniform pillaring of the clay layers.

The PILC samples were then ground and pressed into self-supporting wafers of mass 20–30 mg and placed in an infrared cell. Prior to pyridine adsorption, the wafers were activated in two stages, by dynamic vacuum dehydration at room temperature followed by calcination at 773 K in an oxygen atmosphere for 2 h. The oxygen was removed under dynamic vacuum at 773 K, and the samples were cooled to room temperature. Each wafer was saturated with pyridine by exposure to pyridine vapor (typically, 27 kPa of pyridine at 298 K) for 2 h after which, excess pyridine vapor was removed under dynamic vacuum until the residual pressure dropped to 10^{-7} kPa. Infrared desorption studies were then carried out in which the coverage of the PILC surface was reduced in stepwise fashion under dynamic vacuum at increasing temperatures from a saturated surface until no more pyridine was detected. All spectra were recorded at room temperature. Desorption of pyridine under the static vacuum of the cell was observed to be negligible.

The key IR bands, along with their site and mode assignments, which were employed in this investigation are summarized in Tables II and III. Bands (given with aromatic-ring mode assignments)[26-28] at 1444–1456 cm^{-1} (mode 19b) and 1490–1494 cm^{-1} (mode 19a) were employed in the determination of relative populations of Lewis-pyridine species. Bands at 1540–1550 cm^{-1} (mode 19b and indicative of pyridinium ion) and 1490–1494 cm^{-1}

Table I. Physicochemical Properties of the Pillared Clays Used in This Work

sample	$[M^{n+}]$, mmol g^{-1}	d_{001}/Å[a] 298 K	533 K	873 K[a]	surface area 373 K[b]	613 K[c]
Al–M	2.0	19.4	18.4	9.9	188	167
	4.0	19.5	18.5	9.9	228	206
	6.0	19.6	18.8	16.8	304	285
Al–R	2.0	28.7	27.4	27.2	73	79
	4.0	31.1	27.9	27.7	159	176
Al–SMM	2.0	10.8	10.9	no	159	194
	4.0	11.1	10.3	no	166	218
Zr–M	5.6	18.4	16.9[d]	no	237	194
Zr–R	3.4	38.7	31.8[d]	no	118	151
Ti–M	70.0	diffuse			475	259
Ti–R	23.0	diffuse			263	206
Na–M	0.0	14.8	9.9	9.5	17	26
Na–R	0.0	24.9	19.6	19.2	30	no
Na–SMM	0.0	11.3	10.7	9.7	93	107

[a] Heated 2 h in air. [b] Heated 23.3 h. [c] Heated 76.5 h. [d] 673 K. [e] no = not observed.

Table II. Dominant Infrared Band Positions for Pyridine Adsorbed on Various Oxide Surfaces[a]

mode	19b	19a	8b	8a	refs
liquid	1439	1482	1572	1580	28
PyH+	1540	1490	1640	1620	1
Py·BH_3	1465	1490	1583	1632	1
SiO_2	(P)1466	n.o	(P)1581	(H)1597	50
MgO	(P)1442	(P)1484	(P)1573	(H)1598	52
α-Al_2O_3	(L)1449	(L)1490	(L)1577	(L)1615	51
γ-Al_2O_3	(L^1)1452	(L^1)1494	(L^1)1579	(L^1)1616	51
	(L^2)1455	(L^2)1494	(L^2)1579	(L^2)1624	
η-Al_2O_3	(L^1)1453	(L^1)1496	(L^1)1583	(L^1)1622	1
	(L^2)1457	(L^2)1496	(L^2)1583	(L^2)1632	
ZrO_2	(L)1444	(L)1489	(L)1575	(L)1606	46
			(B)1640		
TiO_2 (anatase)	(L)1445	(L)1494	(L)1575	(L)1613	47

[a] P = physisorbed pyridine. H = hydrogen-bonded pyridine. L = Lewis-bound pyridine. B = Brönsted-bound pyridine. no = not observed.

(23) Ward, J. W. *J. Catal.* **1968**, *11*, 271.
(24) Kukkudapu, R. K.; Kevan, L. *J. Phys. Chem.* **1988**, *92*, 6073.
(25) Young, L. Ph.D. Thesis. University of Auckland, New Zealand, 1991, and references therein.
(26) Turkevich, J.; Stevenson, P. C. *J. Chem. Phys.* **1943**, *11*, 328.
(27) Kline, C. H., Jr.; Turkevich, J. *J. Chem. Phys.* **1944**, *12*, 300.
(28) Corrsin, L.; Fax, B. J.; Lord, R. C. *J. Chem. Phys.* **1953**, *21*, 1170.

Table III. Dominant Infrared Band Positions for Pyridine Adsorbed on Various PILCs after Desorption at Elevated Temperatures[a]

mode	19b	19a	8b	8a	ref
NaM	(L)1445	(L)1491	n.o	(L)1603	this work
NaR	(L)1453	(B,L)1491		(L)1615	
	(B)1545		(B)1639		
NaSMM	(L)1456	(B,L)1491		(L)1621	
	(B)1546		(B)1639		
AlM	(L)1455	(L)1495		(L)1623	
	(B)1549	(B)1492	(B)1640		
AlR	(L)1456	(L)1498		(L)1635	
	(B)1547	(B)1492	(B)1640		
AlSMM	(L)1457	(B,L)1491		(L)1624	
	(B)1548		(B)1640		
ZrM	(L)1445	(B,L)1491		(L)1610	
	(B)1547		(B)1639		
ZrR	(L)1449	(B,L)1491		(L)1611	
	(B)1548		(B)1639		
TiM	(L)1447	(B,L)1491	(L)1575	(L)1613	
	(B)1547	(L)1475	(B)1640		
TiR	(L)1448	(L)1475	(L)1575	(L)1610	
	(B)1547				

[a] P = physisorbed pyridine. H = hydrogen-bonded pyridine. L = Lewis-bound pyridine. B = Brönsted-bound pyridine. no = not observed.

(mode 19a) were employed in the determination of relative populations of pyridine bound to Brönsted sites. Peak IR absorbance values used in the calculation of absorbance ratios were obtained by multiple point baseline correction of spectra, followed by offsetting the baseline to zero absorbance and finally, determination of the maximum absorbance of each corrected band. To account for inconsistencies in density and spectral path lengths of different sample wafers, all bands used site population analyses were normalized against the clay lattice Si-O combination band[29] at 1860–1880 cm^{-1}.

Equipment. A Digilab FTS-60 Fourier transform infrared spectrometer fitted with a DTGS detector was employed in this study. Each spectrum was generated from 32 co-added scans at 2 cm^{-1} resolution. The infrared cell used, with simple modifications, has been previously described.[30] This cell, which incorporated NaCl windows, allowed sample activation, adsorption, heating, and evacuation to be performed without disturbing the sample.

Spectral manipulation and calculation of band intensity information was performed using Spectracalc (Galactic Industries Corp., 1988) software.

Calculation of [Brönsted]/[Lewis] ([B]/[L]) Ratios. The calculation of [B]/[L] ratios uses the data directly from the normalized band absorbances shown in Figures 2–7a. This method of direct calculation does not take into account the extinction coefficients of the two IR bands (*viz.* 19b: 1455 cm^{-1}, 1545 cm^{-1}) employed in the [B]/[L] ratio determination. Thus the data given in Figures 2–7b are displayed as K[B]/[L] where K is a numerical factor determined by the ratio of extinction coefficients. Values for the extinction coefficient ratio $\epsilon^{B}_{1490}/\epsilon^{L}_{1490}$ have been determined for pyridine adsorbed on various oxides,[31-34] but it was found that for pyridine adsorbed on PILCs, values for this coefficient were uncertain. Consistent values for the extinction coefficients of the 19b IR bands were not found in the literature, and thus a truly rigorous analysis was not possible. Nevertheless, the analysis that is presented here provides insight into the behavioral trends of the Brönsted and Lewis surface acid sites on a variety of PILCs.

Liquid nitrogen temperature N_2 adsorption BET surface areas were measured using a fully automated Micromeritics ASAP 2400 which had a maximum *in situ* degassing temperature of 613 K.

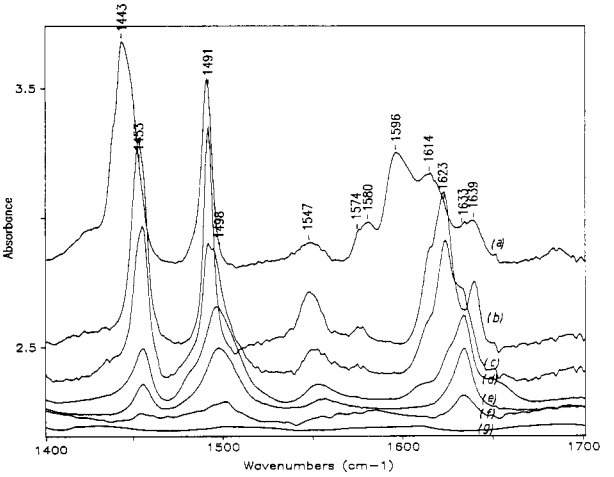

Figure 1. IR spectra of pyridine adsorbed on Al–R. Resolution = 2 cm^{-1}. Desorption temperatures: (a) 298, (b) 473, (c) 573, (d) 673, (e) 773 (f) 873 K; (g) spectrum of activated Al–R before pyridine adsorption.

XRD patterns were obtained using a semiautomated Philips 1640 X-ray diffractometer with Cu Kα radiation.

Results and Discussion

The desorption study was conducted using a PILC surface which was initially saturated with pyridine and which exhibited spectra indicative of at least four types of pyridine: liquid like (condensed) pyridine, physisorbed (P) or hydrogen-bonded (H)-pyridine, Brönsted (B)-pyridine, and Lewis (L)-pyridine. Evidence is also presented in the unpillared systems for a fifth type of surface pyridine, viz., pyridine on exchanged cation sites. A detailed set of pyridine band data is presented in Table III. Bands which coincided with those for liquid pyridine were assigned to condensed (liquidlike) pyridine, and a further class of bands associated with easily desorbed material were attributed to physisorbed pyridine. Figure 1 illustrates a typical pattern of spectral changes, with increasing desorption temperature, for the example of pyridine adsorbed on alumina-pillared rectorite (Al-R4).

The acid-site investigation in this work was based on PILCs activated at 773 K. Therefore in the present study, the temperature-dependent conversion of some Bronsted to Lewis sites which has been reported for uncalcined and steamed PILCs[21] and zeolites[35] is assumed to have already occurred during activation.

(a) Unpillared Sodium Montmorillonite (Na–M). The spectra of surface pyridine following partial desorption at various temperatures reveals that the internal surfaces of the unpillared sodium-ion-exchanged montmorillonite are only weakly acidic. The room temperature spectrum shows physisorbed pyridine dominating the spectrum. However, the BET surface area of Na–M is very small (Table I) and as a consequence, the amount of pyridine adsorbed onto the surface and the observed band absorbances were relatively low. In the room-temperature spectrum physisorbed pyridine dominates the spectrum with bands at 1440, 1489, 1582, 1592, and 1615 cm^{-1}. A band due to Na^+-bound pyridine was observed at 1574 cm^{-1}. After heating at 373 K, only L-pyridine bands at 1445 and 1603 cm^{-1} and the coincident L + B band at 1491 cm^{-1} (see Table III) were observed. After sample des-

(29) Basila, M. R. *J. Phys. Chem.* **1962**, *66*, 2223.
(30) Bartlett, J. Ph.D. Thesis, University of Newcastle, Australia, 1987.
(31) Basila, M. R.; Kantner, T. R. *J. Phys. Chem.* **1966**, *70*, 1689.
(32) Hughes, T. R.; White, H. M. *J. Phys. Chem.* **1967**, *71*, 2192.
(33) LeFrancois, M.; Malbois, G. *J. Catal.* **1971**, *20*, 350.
(34) Sayed, M. B.; Kydd, R. A.; Cooney, R. P. *J. Catal.* **1984**, *88*, 137.
(35) Ward, J. W. *J. Catal.* **1968**, *11*, 238.

orption for 2 h at 473 K the L-pyridine bands almost disappeared leaving only a very weak shoulder at 1445 cm^{-1} and a weak band at 1491 cm^{-1}. After desorption at 573 K the bands due to L-pyridine are no longer detected. This work showed that the surface of Na–M is only weakly acidic with weak Lewis acidity and no Brönsted acidity being observed.

(b) Unpillared Rectorite (Na–R). There is a significant difference in the iron contents of rectorite and montmorillonite,[12] with the former having significantly more iron substitution in the octahedral layers than the latter. The surface area of Na–R (30 $m^2 g^{-1}$), while still low, was higher than that of Na–M (Table I). The spectra of pyridine adsorbed on Na–R were similar but more intense than those of pyridine adsorbed on Na–M. The room-temperature spectrum was dominated by physisorbed pyridine with bands at 1440, 1490, 1582, and 1593 cm^{-1}. A band indicative of Na–pyridine was observed at 1575 cm^{-1}. As in the case of Na–M, the dominant type of acidity evident in the spectra was Lewis type, as reflected in the appearance of a strong 19b band at 1450 cm^{-1}, a strong 19a mode at 1491 cm^{-1} and a weak band at 1621 cm^{-1}. The band at 1450 cm^{-1} is assigned to Al^{3+}–pyridine. Weak B-pyridine bands were observed at 1545 and 1640 cm^{-1} (Table III) and a lower wavenumber component of the 1491 cm^{-1} (19a) band was also detected. After sample desorption at 373 K all evidence for B-pyridine had disappeared, and after sample desorption at 573 K the 1450-cm^{-1} Lewis band also disappeared. At the same time, a new band appeared in the spectrum at 1472 cm^{-1} and the L-pyridine 19a band (1498 cm^{-1}) disappeared. This new band is ascribed to the 19b mode of strongly coordinated Fe^{3+}–pyridine.[35] This assignment was confirmed when bands were detected (see later) at 1472 and 1475 cm^{-1} in spectra of pyridine on Al–R, Ti–M, and Ti–R.

(c) Unpillared Synthetic Mica–Montmorillonite (Na–SMM). The spectra of pyridine adsorbed on Na–SMM differed slightly from those of pyridine adsorbed on Na–M and Na–R in that significant Brönsted acidity was observed (Table III). The dominant species in the room temperature spectrum was physisorbed pyridine with bands at 1438, 1445 (H-bonded pyridine), 1581, and 1600 cm^{-1} being exhibited. After heating to 373 K the dominant type of acidity was Lewis-type with intense absorption bands assigned to L-pyridine detected at 1456 and 1621 cm^{-1}. Significant Brönsted acidity was observed with bands at 1546 and 1639 cm^{-1} being detected. Weak L-pyridine bands persisted after sample desorption at 673 K while the B-pyridine bands were not evident for samples heated above 573 K. The adsorption-induced wavenumber shifts for the L-pyridine bands were similar for both Na–M and Na–SMM, indicating that the Lewis adsorption sites were very similar in character.

The major difference between Na–M, Na–R, and Na–SMM involved the existence of B sites of significant strength on the Na–SMM surface. B-pyridine bands were observed for Na–SMM after desorption at 473 K, whereas Na–M and Na–R did not exhibit any B acidity beyond 373 K. A possible source for the increase in Brönsted acidity of Na-SMM over Na–M and Na–R arises from the conditions employed in the synthesis of this artificial clay. Fluoride is used in the reaction mixture creating some F^- for OH^- substitution in the final product. A recent ^{19}F MAS NMR study of SMM and other layer silicates by Huve *et al.*[36] has determined that the F atom in SMM is bound to two Al atoms and to a lattice vacancy. These substitutions increase the acidity of neighboring hydroxyls because of the higher electronegativity of F, resulting in the withdrawal of electron density from nearest neighbour Al–OH groups making them more acidic. Thus B-pyridine persisted to higher desorption temperature on Na–SMM than Na–M and Na–R.

(d) Alumina-Pillared Montmorillonite (Al–M). When montmorillonite is pillared with aluminum oxyhydroxy species represented[37] in simplified form as (Al_{13}), the surface acidity is greatly enhanced relative to the unpillared clay. This increase in acidity was shown in the IR spectra of pyridine adsorbed on Al–M which showed intense pyridine band absorbances indicating much greater numbers of surface acid sites than for the unpillared clays and increases in pyridine retention and vibrational band shifts suggesting increases in surface acid site strengths. The increase in the number of surface acid sites was assumed to be due to the following factors: an increase in the surface area of the PILC over the parent clay and the availability of new acid sites on the pillars and at pillar–layer bonding sites.

Strong bands assigned to L-pyridine (1453 cm^{-1} and 1623 cm^{-1}), B-pyridine (1549 cm^{-1} and 1640 cm^{-1}) and L+B-pyridine (1491 cm^{-1}) were observed in the spectra of pyridine adsorbed on Al–M (Table III). The L-pyridine bands for higher pillar density Al–M6 still exhibited significant absorbance after sample desorption at 773 K, while the B-pyridine bands disappeared after sample desorption at 773 K (Figure 2A). The extent to which acid sites retain adsorbed pyridine at elevated temperatures reflects the acid strength of a surface site. When the pillar density was increased, both the strength and the numbers of both types of acid site appeared to increase as was reflected in greater relative pyridine band absorbances over all desorption temperatures for Al–M6 than for Al–M4.

The plots in Figure 2B show changes in the relative K[B]/[L] ratios for the two Al–M samples. The Brönsted site strength was generally enhanced with increased pillar density, indicated by the higher overall values of the K[B]/[L] ratios. The sharp decrease in B-pyridine population observed at 573 K for lower pillar density Al–M4 was not observed for higher pillar density Al–M6 until desorption at 773 K. If acid sites were present only on the pillar surfaces, then the qualitative forms of the K[B]/[L] plots would have been expected to be similar. A tentative explanation is proposed in which pillar-to-layer bonding sites between apical Al (from the Al_{13} species) and the tetrahedral clay layer create new Brönsted acid sites. This proposed bonding involves the inversion of AlO_4 tetrahedra at sites of substitution or of SiO_4 tetrahedra in the tetrahedral layer, into the interlayer space allowing the now apicial and unsaturated oxygen to react with the apicial Al of the pillar molecule. Such mechanisms for pillar-to-layer interactions in tetrahedrally substituted clays (beidellite, rectorite) have been proposed in several previous studies.[22,38–40] This behavior has been shown to occur only on calcination above 723 K. It was reported

(36) Huve, L.; Delmotte, L.; Martin, M.; Le Dred, R.; Baron, J.; Saehr, D. *Clays Clay Miner.* **1992**, *40*, 186.
(37) Lahav, N.; Shani, U.; Shabtai, J. *Clays Clay Miner.* **1978**, *26*, 107.
(38) Plee, D.; Borg, F.; Gatineau, L.; Fripiat, J. J. *J. Am. Chem. Soc.* **1985**, *107*, 2362.
(39) Sterte, J.; Shabtai, J. *Clays Clay Miner.* **1987**, *35*, 429.

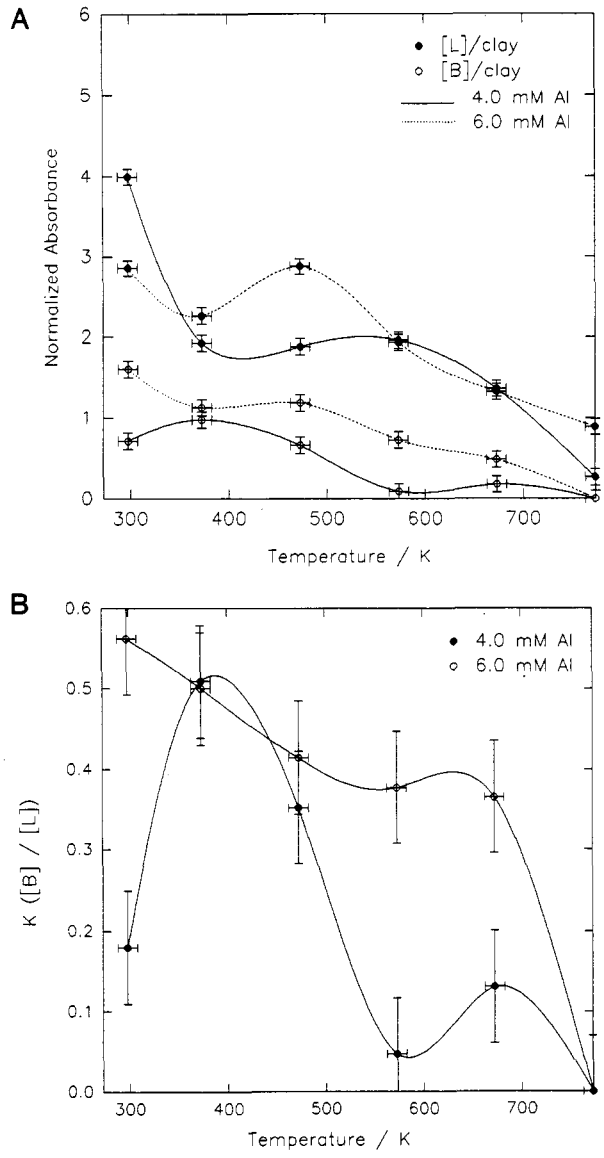

Figure 2. Effect of desorption temperature on L-pyridine and B-pyridine band absorbances for Al–M: (A) normalized against a clay structural unit vibrational band; (B) K[B]/[L] ratios.

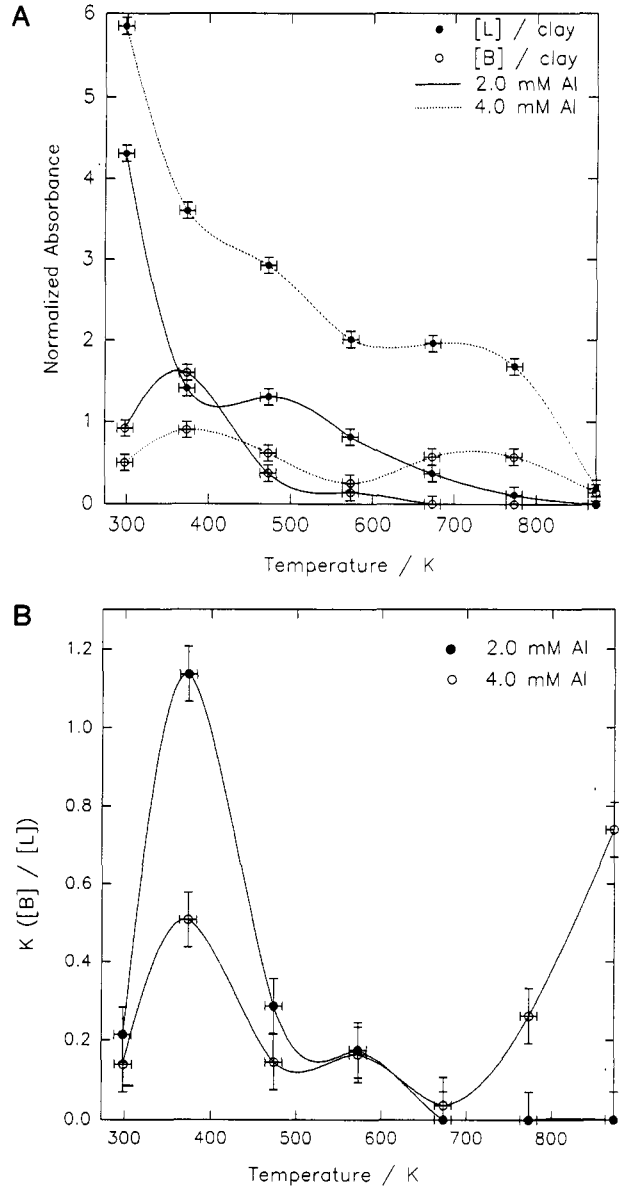

Figure 3. Effect of desorption temperature on L-pyridine and B-pyridine band absorbances for Al–R: (A) normalized against a clay structural unit vibrational band; (B) K[B]/[L] ratios.

in a recent IR and MAS NMR study by Zheng *et al.*[41] that protons were liberated from the pillar precursors on calcination and readily migrated into the clay layers. These protons then protonated the newly formed Al–O–Al or Al–O–Si linkages augmenting the Brönsted acidity of PILCs prepared from tetrahedrally and, as it has since been shown,[41] non-tetrahedrally substituted parent clays. These sites are slightly less favored for pyridine binding because they are both less acidic (furthermore Al–OH–Si will be less acidic than Al–OH–Al) than pillar sites and sterically hindered.[42]

(e) Alumina-Pillared Rectorite (Al–R). The spectra of pyridine adsorbed on Al–R4 (Figure 1), while broadly similar to those of pyridine adsorbed on Al–M, did exhibit some notable differences. The L-pyridine bands for Al–R occurred at higher wavenumbers (1456 and 1635 cm^{-1}) than for Al–M. The bands due to B-pyridine were observed at 1549 and 1640 cm^{-1}, and the coincident 19a band occurred at 1492 cm^{-1} with a component band evident at 1498 cm^{-1} (Table III).

Al–R4 (Figure 3A) and Al–M4 (Figure 2A) exhibited very similar trends in normalized absorbance of both L- and B-pyridine bands. However, unlike Al–M, the separation of [L] and [B] curves for Al–R decreased with decreasing pillar density (*i.e.*, Al–R4 to Al–R2, Figure 3A). A comparison of normalized absorbance curves for Al–PILCs (Figures 2A and 3A) after desorption at 773 K, indicated that Al–PILCs with higher pillar densities have a stronger tendency to retain both B- and L-pyridine.

The K[B]/[L] plot for Al–R2 (Figure 3B) shows ratios decreasing from a peak value of *ca.* 1.2 at 373 K to 0 at 673 K. This behavior indicates an overall decrease in the relative numbers of Brönsted acid sites of Al–R2 over Al–M. The K[B]/[L] plot for Al–R4 shows a steady increase with increasing temperature. Such behavior is consistent with the mechanism discussed earlier to explain the bonding of pillars to the tetrahedral layers of the host clay

(40) Bukka, K.; Miller, L. D.; Shabtai, J. *Clays Clay Miner.* **1992**, *40*, 92.
(41) Zheng, L.; Hao, Y.; Tao, L.; Zhang, Y.; Xue, Z.; *Zeolites* **1992**, *12*, 374.
(42) Guan, J.; Min, E.; Yu, Z. *Proc. 9th. Int. Congr. Catal. Calgary* **1988**, *1*, 104.

which would produce new Brönsted sites in addition to those found on the pillar and clay surfaces. Selected duplicated experiments confirmed these trends were reproducible.

(f) Alumina-Pillared Synthetic Mica-Montmorillonite (Al-SMM). The infrared spectra of pyridine adsorbed on Al-SMM were similar to those previously described for Al-M. However the spectrum of Al-SMM4 displayed a strong, broad band centered at 1440 cm^{-1} which overlapped and obscured the L-pyridine band at 1455 cm^{-1}. The 1440-cm^{-1} band is attributed to pyridine adsorbed on external (nonpillar) alumina-Lewis sites. The external alumina probably formed (during pillaring) as a result of the 3-fold reduction in the pillar capacity of synthetic mica-montmorillonite relative to montmorillonite. This broad band was not present in the spectra of Al-SMM2. The breadth of the band at 1440 cm^{-1} suggested that a number of solid external Al_2O_3 phases were present in the sample. The relatively small increase in surface area (194 to 218 $m^2 g^{-1}$, see Table I) on going from Al-SMM2 to Al-SMM4 may also reflect the presence of external Al_2O_3 formed from excess pillaring solution. The [L]/[clay] curve for Al-SMM4 is not presented (Figure 4A) because of uncertainties occurring from the overlap of the 1440-cm^{-1} band with the L-pyridine band at 1457 cm^{-1} of Al-SMM4. Strong L-pyridine bands were observed in the spectrum of pyridine adsorbed on Al-SMM2 and Al-SMM4 at 1455 and 1635 cm^{-1}, and strong bands assigned to B-pyridine were observed at 1548 and 1640 cm^{-1}. The coincident B + L band was observed at 1491 cm^{-1} (Table III).

The L-pyridine bands for Al-SMM2 and Al-SMM4 decreased steadily in absorbance with increasing temperature. The Al-SMM2 B-pyridine band absorbance decreased similarly with increasing temperature up to 773 K where it was no longer detected and a similar trend was observed for Al-SMM4. While the behavior of the L-sites have been shown to be very similar to Al-M, there is a significant difference in behavior between the B-sites on Al-SMM and Al-M. Because the Lewis acidity seems exclusively to be associated with the pillar surfaces and because of the large numbers of L-sites involved, the behavior of these sites was expected to be similar on all of the Al-PILCs. On the other hand, there are significant numbers of B sites found on the surfaces of the clay layers and at pillar-to-layer junctions. As a result of fluoride-hydroxide substitution, some of the Brönsted sites in SMM exhibited increased acidity relative to those of Al-M or Al-R.

The plot of K[B]/[L] ratios (Figure 4B) shows that the Brönsted acidity of Al-SMM2 was abundant after desorption at room temperature but Lewis acidity dominates after desorption at more elevated temperatures. The data for Al-SMM4 show that Lewis acidity dominated over almost the entire temperature range while the Brönsted acid sites on Al-SMM4 retained pyridine to higher temperatures than those on Al-M (Figure 2A) and Al-R (Figure 3A) indicating the existence of stronger Brönsted sites on the Al-SMM surface. The increased strength of these sites must be influenced, or indeed created, by the F^- for OH^- substitution in the layers of the SMM clay.

(g) Zirconia-Pillared Montmorillonite (Zr-M). The behavior of the surface acid sites on Zr-M has been the subject of only limited study.[43-45] The infrared spectra of

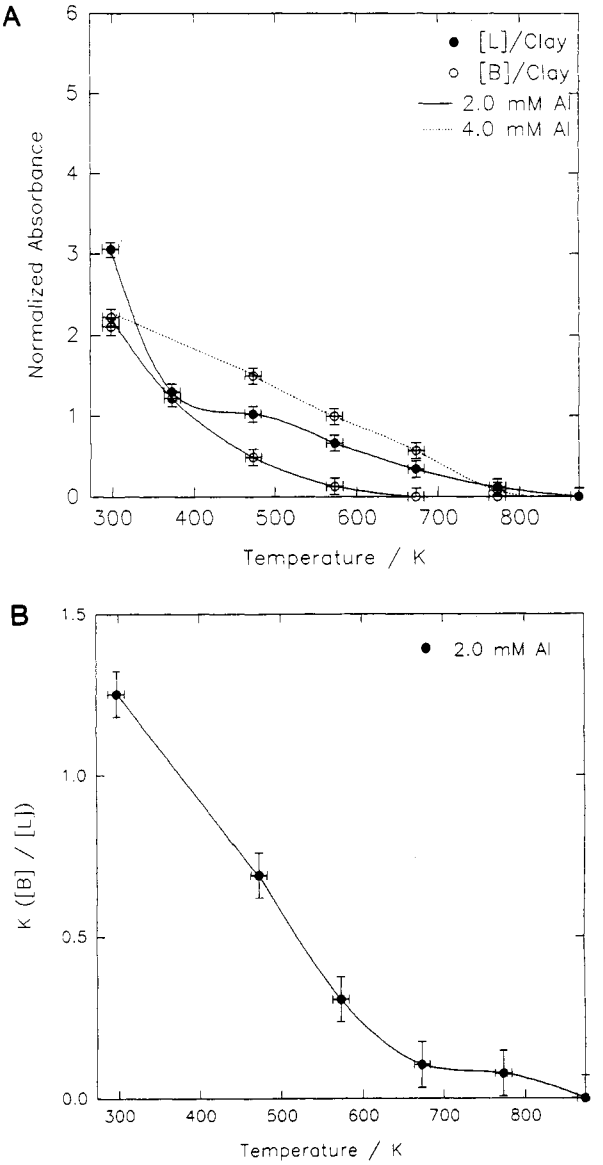

Figure 4. Effect of desorption temperature on L-pyridine and B-pyridine band absorbances for Al-SMM: (A) normalized against a clay structural unit vibrational band; (B) K[B]/[L] ratios.

pyridine adsorbed on Zr-M are similar to those discussed earlier for the Al-PILCs. It was previously reported[44] that the bands arising from pyridine interaction with acid sites on Zr-M occurred at slightly lower frequency than for Al-PILCs. This behavior was observed in the current study, with bands detected at 1445 and 1610 cm^{-1} (L-pyridine) and 1547 cm^{-1} and 1639 cm^{-1} (B-pyridine). The coincident 19a (L+B-pyridine) band shows one component at 1491 cm^{-1}. The adsorption-induced wavenumber shifts for the 19b band, from liquid pyridine (Table II and III) are less for Zr-M (+6 cm^{-1}) than for Al-M (+16 cm^{-1}) indicating that the coordinatively unsaturated Zr^{4+}-Lewis acid site is less electron-withdrawing than the corresponding Al^{3+}-Lewis acid site. The wavenumber shifts for the B-pyridine 19b band for Zr-M (+108 cm^{-1}) and Al-M (+106 cm^{-1}) are similar, suggesting that any available acidic hydroxyls are similar in these two cases. The surface of

(43) Bartley, G. J. J.; Burch, R. *App. Catal.* **1985**, *19*, 175.

(44) Burch, R.; Warburton, C. I. *J. Catal.* **1986**, *97*, 503.

(45) Plee, D.; Gatineau, L.; Fripiat, J. J. *Clays Clay Miner.* **1987**, *35*, 81.

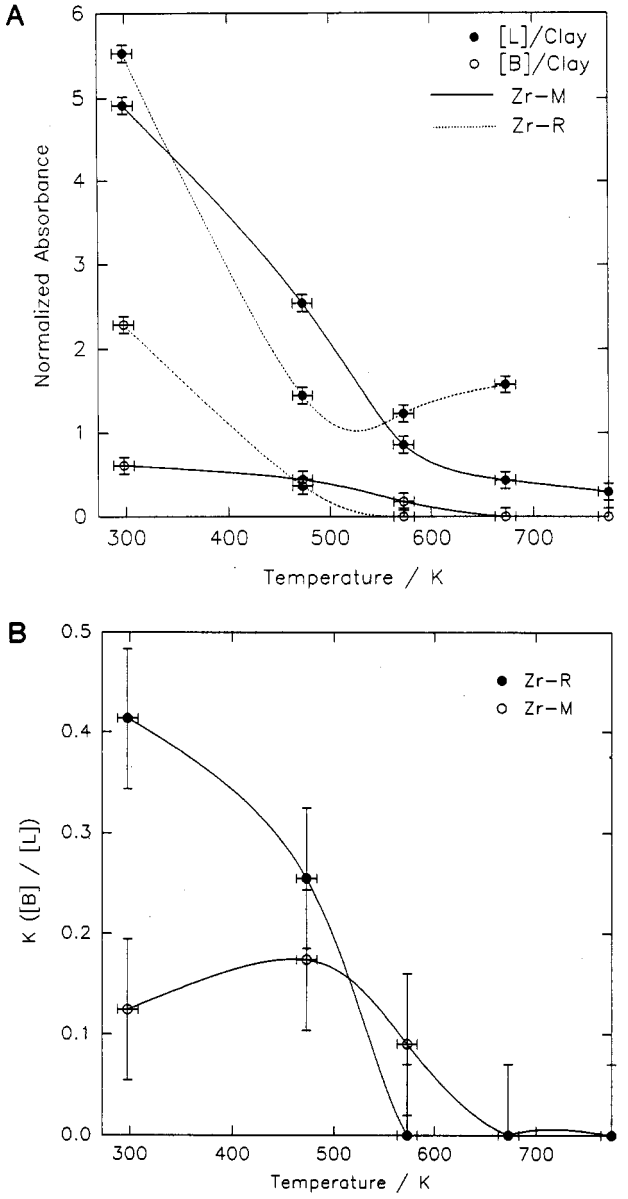

Figure 5. Effect of desorption temperature on L-pyridine and B-pyridine band absorbances normalized against a clay structural unit vibrational band: (A) Zr–M and Zr–R. (B) Effect of desorption temperature on the K[B]/[L] ratios of Zr–M and Zr–R.

ZrO_2 (Table II) has been previously shown to exhibit weak Lewis acidity[46] with L-pyridine bands reported at 1444, 1489, 1575, and 1606 cm^{-1}. In contrast to the significant B-pyridine bands seen in Zr–M, only one weak B-pyridine band at 1640 cm^{-1} was reported for ZrO_2 (see Table II). Thus the current study suggests an enhancement in Brönsted acidity of Zr–M relative to ZrO_2.

The desorption of pyridine from the Zr–M surface shows simple behavior (Figure 5A) with residual Lewis acidity being detected after desorption at 773 K. The B-pyridine spectrum is very weak after desorption at 673 K. The K[B]/[L] ratio (Figure 5B) demonstrates a similar trend to Al–M, where L-acidity appears to be playing the dominant role in determining the acid character of the Zr–M surface. All this data supports the contention that Zr–M Lewis sites (associated with coordinatively unsaturated Zr^{4+} ions) are weaker but more abundant than the

(46) Hertl, W. *Langmuir* **1989**, *5*, 96.

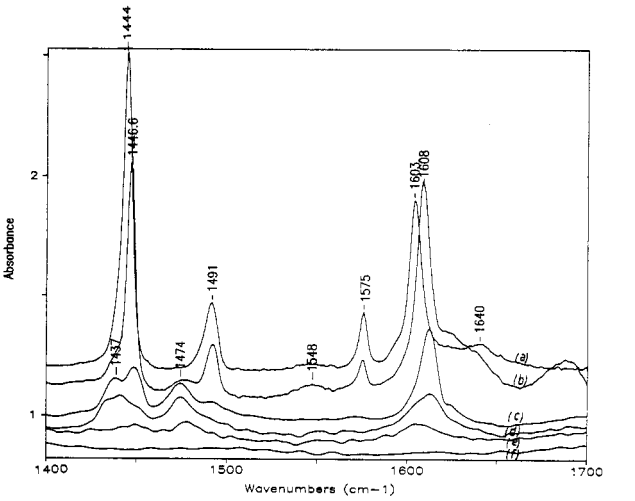

Figure 6. IR spectra of pyridine adsorbed on Ti–M. Resolution = 2 cm^{-1}. Desorption temperatures: (a) 298, (b) 473, (c) 573, (d) 673, (e) 773 K; (f) spectrum of activated Ti–M before pyridine adsorption.

Al–M sites. The slightly larger wavenumber shift for B-pyridine observed on Zr–M over Al–M suggests that the B-acid sites created on Zr–M are slightly more acidic than on Al–M. It is surmised that the Brönsted acidity observed on Zr–M can only be due to clay-layer hydroxyls or to pillar-layer bonding sites. While the Zr^{4+} L-sites were observed to be less acidic than the Al^{3+} L-sites it is nevertheless concluded that Zr–O–Al or Zr–O–Si pillar-layer linkages are slightly more acidic than the corresponding linkages in Al–PILCs. This is due either to the differences in electronegativity of the various atoms in the linkage, or that the Zr–O–clay site may be more accessible to the adsorbate.

(h) Zirconia-Pillared Rectorite (Zr–R). The IR spectra of pyridine adsorbed on a new pillared clay material Zr–R, effectively combined the features of those of Al–R and Zr–M. Bands observed at 1449 and 1611 cm^{-1} were assigned to L-pyridine, while bands observed at 1548 and 1639 cm^{-1} were assigned to B-pyridine (Table III). Hence the L-pyridine 19b band shift (relative to liquid pyridine, see Tables II and III) for Zr–R was +10 cm^{-1} and the B-pyridine 19b band shift for Zr–R was +109 cm^{-1}. Similar differences (*ca.* 3–4 cm^{-1}) between L-pyridine band shifts were observed for Zr–M (+6 cm^{-1}) and Zr–R (+10 cm^{-1}) as for Al–M (+16 cm^{-1}) and Al–R (+19) cm^{-1}). The level of Brönsted acidity for Zr–R, as for Zr–M, was relatively low, and Lewis acidity for both Zr–PILCs decreased sharply after desorption at 573 K (Figure 5A).

The K[B]/[L] ratio (Figure 5B) for Zr–R indicated a higher B-acidity compared to Zr–M at low desorption temperatures which declined sharply after desorption at 573 K. This datum further enhanced the conclusions reached in the Zr–M case, that the L-acidity of Zr-PILCs is weaker than that of the Al–PILCs, but that the Brönsted acidity is slightly stronger than that of Al–PILCs and that the acidity of pillared rectorites is stronger than that of pillared montmorillonites.

(i) Titania-Pillared Montmorillonite (Ti–M). In addition to the bands reported for other PILCs, the infrared spectra of pyridine adsorbed on Ti–M (Figure 6) showed two new bands at 1473 and 1575 cm^{-1}. The band at 1473 cm^{-1} was detected after desorption at 573 K and disappeared during desorption at 773 K. The 1575-cm^{-1} band which was evident at room temperature, disappeared

after desorption at 573 K.

A recent study of pyridine adsorbed onto TiO_2 (anatase), Dines *et al.*[47] reported L-pyridine bands at 1613, 1575, 1494, and 1445 cm^{-1} which they assigned to the 8a, 8b, 19a, and 19b ring vibrations of L-pyridine respectively (Table II). No evidence for B-pyridine bands on pure TiO_2 was found in their work, in agreement with other studies on anatase[48] and silica–titania binary oxides.[49] The L-pyridine bands for pyridine on anatase showed some splitting on heating of the sample.[47] This behavior was explained by the existence of two different types of Lewis site on the anatase surface. The 1575-cm^{-1} band in that study disappeared after desorption at 673 K, as did the same band in the current study. Therefore the band at 1575 cm^{-1} (8b) for the Ti–M case is given a similar assignment, namely, TiO_2 L-pyridine type 1 and may be associated with "extraframework" amorphous TiO_2 that may have been formed during the pillaring procedure. Similarly, the bands at 1447 (19b) and 1612 cm^{-1} (8b) (Figure 6, curve C) are assigned to L-pyridine type 2.

The type 1 Lewis site is the weaker of the two, releasing pyridine at low temperature and producing only a small (+3 cm^{-1}) wavenumber shift from liquid pyridine in the IR spectrum of adsorbed pyridine. Thus the type 1 site is a weak electron acceptor (and hence a weak acid site) thought to be due to singly coordinatively unsaturated Ti^{4+} ions.[47] The stronger site, type 2, although not as strong as those seen on Al–PILCs, is thought to be due to doubly coordinatively unsaturated Ti^{4+} ions.[47] Very weak bands at 1548 and 1640 cm^{-1} are assigned to B-pyridine, and the 1491-cm^{-1} band is assigned to the coincident 19a L+B-pyridine band. The 1491-cm^{-1} band disappears after desorption at 573 K and at the same temperature a band at 1473 cm^{-1} appears. A possible explanation for this band involves the thermal rearrangement of the TiO_2 pillar creating a Ti^{4+} ion of lower coordination, hence stronger acidity. It was not clear whether it was the existing L-pyridine sites that were observed or whether new sites were formed to which the adsorbed pyridine molecules migrated. The very weak B-acidity observed is in agreement with Dines *et al.*,[47] who detected no B-pyridine on the anatase surface, and Morterra *et al.*,[48] who observed pyridinium ion only in the presence of SO_4^{2-} impurities. Thus the weak B-pyridine bands observed here are assigned to acidic hydroxyl groups found in the octahedral layer of the clay platelets and exposed at platelet edges, at fracture sites and at pillar-to-layer junctions. The low absorbance values of these bands are consistent with the very small number of clay surface hydroxyls that would be available for pyridine interaction.

The results given in Figure 7 indicate that the Lewis acid strength and behavior of Ti–M is similar to that of the Zr–M analogue with little L-pyridine being observed after desorption at 773 K and no B-pyridine after desorption at 573 K. The K[B]/[L] plot (Figure 7B) shows that Lewis acidity completely dominates the surfaces of Ti–M.

(j) Titania-Pillared Rectorite (Ti–R). A second novel material in addition to Zr–R was prepared by pillaring Na–rectorite with titanium oxy–hydroxy oligomers. As for other titania PILCs X-ray diffraction patterns were diffuse (Table I) and offered little information (See Experimental Section), but surface area data (263 m^2g^{-1}) indicated that pillaring had occurred. The infrared spectra of pyridine adsorbed on Ti–R and Ti–M were very similar. The pyridine spectrum after desorption at room temperature showed bands due to L-pyridine at 1444 and 1604 cm^{-1}, B-pyridine at 1545 and 1638 cm^{-1}, the L+B-pyridine coincident band at 1491 cm^{-1} and a third pair of weak bands at 1430 and 1575 cm^{-1}. The positions of these bands are in close agreement with the bands in the spectra of pyridine adsorbed on Ti–M (Figure 6).

After desorption at 573 K the 1430- and 1575-cm^{-1} bands disappeared and a band at 1478 cm^{-1} appeared. The 1444- and 1604-cm^{-1} bands shifted to 1448 and 1610 cm^{-1}, respectively, with a general loss of absorbance associated with desorption. The weak B-pyridine bands disappeared after desorption at 473 K (Figure 7A), and the 1491-cm^{-1}

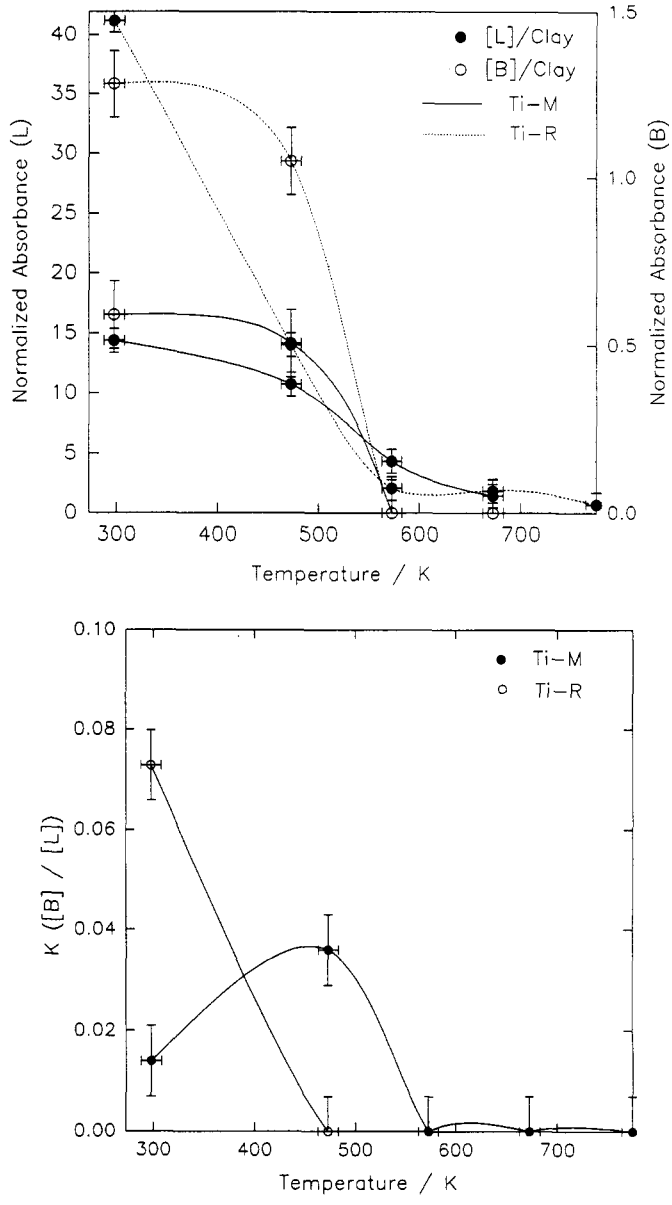

Figure 7. Effect of desorption temperature on L-pyridine and B-pyridine band absorbances normalized against a clay structural unit vibrational band. (A) Ti–M and Ti–R. (B) Effect of desorption temperature on the K[B]/[L] ratios of Ti–M and Ti–R.

(47) Dines, T. J.; Rochester, C. H.; Ward, A. M. *J. Chem. Soc., Faraday Trans. 1* **1991**, *87*, 643.
(48) Morterra, C. *J. Chem. Soc., Faraday Trans* **1980**, *76*, 2102.
(49) Odenbrand, C. U. I.; Brandin, J. G. M.; Busca, G. *J. Catal.* **1992**, *135*, 505.
(50) Connell, G.; Dumesic J. A. *J. Catal.* **1986**, *102*, 216.
(51) Connell, G.; Dumesic, J. A. *J. Catal.* **1986**, *101*, 103.
(52) Martin, C.; Martin, I.; Rives, V. *J. Mol. Catal.* **1992**, *73*, 51.

band disappeared after desorption at 673 K. Band assignments are as follows:[47] 1430 cm^{-1}, strongly H-bonded pyridine; 1444 and 1610 cm^{-1}, type 2 Lewis sites and 1575 cm^{-1}, type 1 Lewis sites. The B-pyridine bands (1547 and 1638 cm^{-1}) are due to pyridine interacting with acidic hydroxyls on the clay surface and at pillar–layer junctions. The assignment of the 1478-cm^{-1} band was complicated by the fact that two different explanations had already been proposed for this band. In the Na–R case a band at 1472 cm^{-1} was ascribed to Fe^{3+}–pyridine, while for Ti–M a band at 1473 cm^{-1} was assigned to a new Ti^{4+} site on the pillar surfaces. This assignment was made because no 1473-cm^{-1} band was observed on Na–M. In the Ti–R case, the preferred assignment in this case is to Fe^{3+}–pyridine.

The argument proposed by Plee *et al.*[45] for Al-pillared beidellite was invoked earlier in this paper for the other Al–PILCs studied and is applied here also to Ti–M and Ti–R. Because of the beidellitic nature of the swelling layers in rectorite, it was expected that the numbers of B-acid sites would be greater for Ti–R than for Ti–M.[45] This was evident in the data in Figure 7A, which shows that the normalized absorbances of the B-pyridine bands of Ti–R, while low, were nevertheless greater than for Ti–M. This is consistent with the knowledge that there are more isomorphous Al for Si substitutions in the tetrahedral layers of rectorite than in montmorillonite. Hence a greater number of pillar-to-layer bonds are expected at these sites of substitution, leading to a greater number of Brönsted acid sites (although not necessarily to an increase in the acid strengths of these sites). The ratio of B-pyridine absorbances for Ti–M to Ti–R (0.5) was not a simple reflection of the ratio of surface areas (1.26) and therefore must correspond to increased B-site population for Ti–R. While the work of Zheng *et al.*[41] suggested that tetrahedral substitution is not essential for pillar–layer bonding, the current study indicates that pillar-to-layer bonding is more likely with tetrahedrally substituted clays. The K[B]/[L] ratios (Figure 7B) show that after desorption at 473 K the Brönsted acid sites have been eliminated and that Lewis acidity dominates. This is consistent with the literature regarding the acidity of TiO_2 surfaces.[47–49] These data indicate that some form of pillar–layer linkage is formed between the Ti pillar and the rectorite layer as was suggested for Al–M and Al–R by Zheng *et al.*[41]

Acknowledgment. The authors would like to thank the Petroleum Research Fund of the American Chemical Society for financial assistance, Professor R. Howe (University of New South Wales), particularly, and Professor P. Black, Ms. S. Courtney and Mr. R. Sims of the Auckland University Geology department for assistance and advice, Drs. John Seakins and Les Young for help with syntheses and interpretation of data, ANSTO Advanced Materials Laboratory, Lucas Heights, Australia, for surface area and pore distribution analyses. S.A.B. would like to thank the New Zealand Ministry of Research, Science and Technology for a Postgraduate study award for Maori students of science and engineering.